https://doi.org/10.5607/en24019
Exp Neurobiol. 2024 Aug;33(4):180-192.
pISSN 1226-2560 • eISSN 2093-8144

Original Article

Experimental Neurobiology

Generation of Astrocyte-specific BEST1 Conditional Knockout Mouse with Reduced Tonic GABA Inhibition in the Brain

Jinhyeong Joo[1,2], Ki Jung Kim[1], Jiwoon Lim[1,2], Sun Yeong Choi[1,3], Wuhyun Koh[1] and C. Justin Lee[1,2*]

[1]Center for Cognition and Sociality, Institute for Basic Science (IBS), Daejeon 34126,
[2]IBS School, Korea University of Science and Technology (UST), Daejeon 34113,
[3]Department of Biomedical Engineering, Ulsan National Institute of Science and Technology (UNIST), Ulsan 44919, Korea

Bestrophin-1 (BEST1) is a Ca^{2+}-activated anion channel known for its role in astrocytes. Best1 is permeable to gliotransmitters, including GABA, to contribute to tonic GABA inhibition and modulate synaptic transmission in neighboring neurons. Despite the crucial functions of astrocytic BEST1, there is an absence of genetically engineered cell-type specific conditional mouse models addressing these roles. In this study, we developed an astrocyte-specific BEST1 conditional knock-out (BEST1 aKO) mouse line. Using the embryonic stem cell (ES cell) targeting method, we developed *Best1* floxed mice (C57BL/6JCya-*Best1*^{em1flox}/Cya), which have exon 3, 4, 5, and 6 of *Best1* flanked by two loxP sites. By crossing with hGFAP-CreER^{T2} mice, we generated *Best1* floxed/hGFAP-CreER^{T2} mice, which allowed for the tamoxifen-inducible deletion of *Best1* under the human GFAP promoter. We characterized its features across various brain regions, including the striatum, hippocampal dentate gyrus (HpDG), and Parafascicular thalamic nucleus (Pf). Compared to the Cre-negative control, we observed significantly reduced BEST1 protein expression in immunohistochemistry (IHC) and tonic GABA inhibition in patch clamp recordings. The reduction in tonic GABA inhibition was 66.7% in the striatum, 46.4% in the HpDG, and 49.6% in the Pf. Our findings demonstrate that the BEST1 channel in astrocytes significantly contributes to tonic inhibition in the local brain areas. These mice will be valuable for future studies not only on tonic GABA release but also on tonic release of gliotransmitters mediated by astrocytic BEST1.

Key words: Astrocyte, BEST1, Gamma-aminobutyric acid, Striatum, Hippocampus, Thalamus

INTRODUCTION

Bestrophin 1 (BEST1) is a Ca^{2+}-activated Cl^- channel, first discovered in retinal pigment epithelium, and over 250 mutations of BEST1 are known as causes of bestrophinopathies [1, 2]. BEST1 is now reported to be expressed throughout the brain [3], including the cerebellum [4], striatum [5], hippocampus [6], cerebral cortex [7], thalamus [8], dorsal root ganglia [9, 10] and spinal cord [11]. BEST1 is primarily localized in microdomains of astrocytes [3] and contributes to controlling astrocytic volume transient [12] and modulating synaptic activity by releasing GABA [4], glutamate [6, 13-15], and D-serine [16] from astrocytes. Astrocytic GABA release has an essential physiological role via tonic inhibition for neuronal information processing [17], like controlling sensory acuity in the thalamus [8] and motor coordination in the cerebellum [18]. In pathophysiological conditions such as Alzheimer's disease [19] and Parkinson's disease [20], astrocytes become reactive and suppress neighboring neurons with severe tonic inhibition [21]. Moreover, it is reported that redistribution of BEST1 expression can occur in reactive astrocytes of Alzheimer's disease [21]. Although the importance of the BEST1 channel in astrocytic gliotransmission has been recognized, BEST1 null knockout cannot directly explain astrocytic tonic GABA release since BEST1 is revealed to be expressed in both neurons and astrocytes [22].

Submitted August 15, 2024, Revised August 29, 2024,
Accepted August 31, 2024

*To whom correspondence should be addressed.
TEL: 82-42-878-9150, FAX: 82-42-878-9151
e-mail: cjl@ibs.re.kr

Therefore, genetically engineered mouse models are needed to study the astrocytic BEST1 channel solely. We generated a new astrocyte-specific BEST1 conditional knockout (BEST1 aKO) mouse line to address this.

To generate a conditional BEST1 knockout mouse line, we first established a *Best1* floxed mouse line using the ES cell targeted method, a gold standard gene editing technique [23]. Exons 3 to 6 of the *Best1* gene were targeted for flanking with the loxP site, creating a target vector. The targeting vector provides the necessary homology arms to facilitate recombination at the desired genomic locus, and successful recombination events are identified through selection and screening. The ES cell targeting method has a lower success rate but does not introduce specific DNA damage, unlike techniques such as CRISPR, ZFNs, or TALENs [24-26]. Moreover, it relies on the cell's mechanisms to make precise genetic changes, avoiding problems like off-target effects.

To study BEST1 in astrocytes specifically, we crossed the *Best1* floxed mouse line with a Cre-expressing mouse line driven by an astrocytic promoter. While the ALDH1L1-CreER^{T2} mouse line offers more pan-astrocyte-specific expression, its broad utility for brain-specific research is severely limited by the ubiquitous expression of *Aldh1l1* mRNA throughout the body [27]. We opted to use the tamoxifen-inducible hGFAP-CreER^{T2} system for targeting astrocyte-specific BEST1. We examined BEST1 and GABA expression and tonic GABA release in astrocytes of the striatum, hippocampal dentate gyrus (HpDG), and Pf using IHC and brain slice patch-clamp techniques. In the striatum, HpDG, and Pf of the BEST1 aKO mouse, we found significantly reduced BEST1 expression and tonic GABA inhibition compared to the Cre-negative control, validating conditional deletion of BEST1 in astrocytes.

MATERIALS AND METHODS

Animals

Both male and female mice were used in this study. Mice were given *ad libitum* access to food and water, maintained under a 12:12 hour light-dark cycle, and housed in groups of 3~5 per cage. All care and handling of mice were conducted according to protocols approved by the Institutional Animal Care and Use Committee (IACUC) of the Institute for Basic Science (Daejeon, South Korea).

Generation of Best1 floxed mouse line

The generation of a *Best1* floxed mouse line was commissioned from Cyagen Biosciences (Guangzhou, China). The floxed allele of *Best1* was engineered using a technique based on the ES cell targeting method. This involved the amplification of mouse genomic fragments containing homology arms and a conditional knockout region from a Bacterial Artificial Chromosome (BAC) clone with high-fidelity Taq DNA polymerase. These fragments were subsequently integrated into a target vector that included recombination sites. The vector also incorporated a neomycin resistance gene cassette, bordered by self-deletion anchor sites to facilitate positive selection. This construct was then linearized and introduced into C57BL/6-derived ES cells via electroporation. Following homology-directed recombination, these cells underwent selection using neomycin and were further validated by Southern blot. Selected ES cells were microinjected into blastocysts and transferred into pseudopregnant females, yielding chimeric progeny. These chimeric mice were crossed with wild-type mice to produce heterozygous offspring, which were subsequently bred to achieve homozygosity. *Best1* floxed mice harbored the modified allele with loxP sites flanking exons 3 through 6. According to the nomenclature guidelines for genetically engineered mice by the International Committee on Standardized Genetic Nomenclature for Mice, this line was named C57BL/6JCya-*Best1*^{em1flox}/Cya.

Generation of BEST1 aKO mouse line

Homozygous *Best1* floxed mice was crossed with transgenic hGFAP-CreER^{T2} (B6-Tg(GFAP-cre/ERT2)13Kdmc, Cre/+) mice to generated *Best1* floxed/hGFAP-CreER^{T2} mice. To generate astrocyte-specific *Best1* knockout (BEST1 aKO), adult (aged 8~11 weeks) *Best1* floxed/hGFAP-CreER^{T2} (Cre/+ or +/+ as control) mice were injected with tamoxifen (100 mg/kg) once per day for five days by intraperitoneal route. Tamoxifen was dissolved in sunflower oil containing 10% ethanol at a concentration of 20 mg/ml. Mice were used for IHC or electrophysiological experiments at least two or three weeks later for the robust CreER^{T2} system activation.

Genotyping

The mouse tail was submerged into a mixture of 1 mg/ml proteinase K (21560025-2, bioWORLD, USA) and tail lysis buffer (102, Fiat international, South Korea) and digested overnight at 65°C. The next day, proteinase K was inactivated at 85°C for 1 hour. Extracted genomic DNA was genotyped by taking a supernatant from the tail lysate. The PCR mixture for *Best1* floxed mouse DNA contained 2×PCR premix reagent (QM13531, Bioquest, South Korea), 3 μl of genomic DNA template, 1 μl of primer sets (10 pmol/μl), and 5 μl of distilled water (D.W.). The PCR mixture for GFAP CreER^{T2} mouse DNA contained 2X PCR premix reagent, 3 μl of genomic DNA template, 0.5 μl of primer sets (10 pmol/μl), and 6 μl of D.W. For *Best1* floxed mice, genotyping was performed by PCR using the following two pairs of primers to target each upstream

and downstream loxP site.

Pair 1
Forward #1 (F1), 5'-CCACACACCTTTACTTCTACCCC-3'
Reverse #1 (R1), 5'-TACTATACCATCGTTGTGTGGCTGG-3'

Pair 2
Forward #2 (F2), 5'-AGACACACACGGTCCAGAACTG-3'
Reverse #2 (R2), 5'-ATCGGTCTATTGTTGCCACTGCC-3'

PCR using F1, R1 primer performed by the following cycling protocol: 94°C for 3 min, 33 cycles of 94°C for 30 sec, 62°C for 35 sec, 72°C for 35 sec, with the final extension step, 72°C for 5 min. PCR using F2, R2 primer performed by the following cycling protocol: 94°C for 3 min, 35 cycles of 94°C for 30 sec, 62°C for 35 sec, 72°C for 35 sec, with the final extension step, 72°C for 5min. For the GFAP-CreER^{T2} mouse, genotyping was performed by PCR using the following primers based on the previous report [28]:

Pair 1
hGFAP_F: 5' - AGACCCATGGTCTGGCTCCAGGTAC - 3'
BAC_R: 5' - ACTGACATTTCTCTTGTCTCCTC - 3'

Pair 2
BAC_F: 5' - ATCGCTCACAGGATCACTCAC - 3'
CreERT2_R: 5' - TCCCTGAACATGTCCATCAGGTTC - 3'

WT primer
Intron3_WT_R: 5' - CTAGCTGGTAAGTTGTGTGTGTC - 3'

PCR using hGFAP_F, BAC_R, BAC_F, CreERT2_R, and Intron3_WT_R primer performed by the following cycling protocol: 95°C for 5 min, 33 cycles of 95°C for 30 sec, 58°C for 30 sec, 72°C for 30 sec, with the final extension step, 72°C for 4 min. PCR products were run on 1.5% and 2% agarose gels (HB0100500, E&S, South Korea) in TAE buffer (40 mM Tris, pH 7.6 with 20 mM acetic acid and 1 mM EDTA) at 100 V for 25 min and visualized using a non-harmful nucleic acid staining solution, RedSafe (21141, iNtRON Biotechnology, South Korea).

Sanger sequencing for detection of loxP sites

The upstream loxP site near exon 3 was amplified by PCR using F1 and R1 primer with the same genotyping protocol. Homozygous *Best1* floxed mouse DNA was used, confirmed by gel electrophoresis that the amplified DNA has a 283 bp band. The downstream loxP site near exon 6 was amplified by PCR using F2 and R2 primer with the same protocol. Homozygous *Best1* floxed mouse DNA was used, confirmed by gel electrophoresis that the amplified DNA has a 259 bp band. Cosmogenetech (Daejeon, South Korea) conducted a DNA clean-up of PCR product and Sanger sequencing.

Immunohistochemistry

The mouse was anesthetized with 1~2% isoflurane, then transcardiac perfused with saline and 4% paraformaldehyde (PFA). The brain was detached and immediately submerged into 4% PFA for post-fixation at 4°C overnight. Subsequently, the brain was transferred into a 30% sucrose solution for cryoprotection and stored at 4°C. Brain tissue was frozen at -70°C and sectioned with 30 μm thickness in the coronal plane in a cryostat (CM1950, Leica Biosystems, Germany). For the brain tissue immunostaining, brain sections were incubated in a blocking solution containing 0.3% Triton X-100 (X100, Sigma-Aldrich, USA), 4% donkey serum (GTX27475, Genetex, USA), and 0.1M PBS. Then, sections were immunostained with optimized concentrations of primary antibodies (Custom-made Rabbit anti-BEST1, GWVitek, South Korea, antigen: C-AESYPYRDEAGTKPVLYE (19mer), 1:250; Guineapig anti-GABA, ab175, Millipore, Germany, 1:250; Mouse anti-S100β, S2532, Sigma-Aldrich, USA, 1:250) in blocking solution at 4°C overnight. After washing with 0.1 M PBS three times, secondary antibodies with corresponding fluorescent in blocking solution were applied for two hours to brain sections, then washed thoroughly with 0.1 M PBS three times. DAPI (62248, Thermo Fisher Scientific, USA; 1:1000) was added during the second wash to stain the nucleus. Secondary antibodies were purchased from Jackson Immuno Research Laboratories (USA). Brain sections were mounted at silane-coated slide glass (5116-20F, Muto Pure Chemicals, Japan) with Fluorescence mounting medium (S3023, Dako, Denmark). The fluorescent image was acquired by Zeiss LSM900 confocal microscope, with Z-stacked in 1 μm intervals.

Image quantification

Fluorescent images obtained from confocal microscopy were analyzed using ImageJ Fiji (NIH, USA). To quantify GABA and BEST1 immunoreactive intensity, all images were z-stacked with max intensity by pixel, set at the same brightness and contrast. The region of interest (ROI) was set by calculating the area of S100β with the same threshold setting throughout the whole image. S100β-positive GABA and BEST1 intensity in each ROI was analyzed in 8-bit images. To quantify the neuronal BEST1 expression level in the Pf, the S100β-negative, BEST1-positive region around DAPI was selected for ROI. BEST1 intensity in neuron-shaped ROI was calculated.

https://doi.org/10.5607/en24019

Brain slice preparation

Animals were anesthetized with 1.5~2% isoflurane and decapitated to isolate the brain. The mouse skull was directly submerged into ice-cold high sucrose artificial cerebrospinal fluid (aCSF) (in mM): 26 $NaHCO_3$, 1.25 NaH_2PO_4, 3 KCl, 5 $MgCl_2$, 0.1 $CaCl_2$, 10 D(+)-glucose, and 212.5 sucrose, pH 7.4. After slicing, brain slices were cut at 300 μm thick in horizontal plane using a vibratome (DSK Linear Slicer, Kyoto, Japan) and stored into aCSF (in mM): 130 NaCl, 24 $NaHCO_3$, 1.24 NaH_2PO_4, 3.5 KCl, 1.5 $CaCl_2$, 1.5 $MgCl_2$, and 10 D(+)-glucose, pH 7.4 at room temperature for at least one hour for recovery before recording. All solution was oxygenated for at least one hour by aerating mixed gas containing 95% O_2 and 5% CO_2.

Slice recording for tonic GABA current

Slices were placed in a recording chamber, and target cells were identified using an upright Zeiss microscope equipped with a 60× water immersion objective and infrared differential interference contrast (DIC) optics. Whole-cell recordings were conducted at room temperature using pCLAMP11 software, a Digidata 1550B, and a MultiClamp 700B amplifier (Axon Instrument, Molecular Devices). We performed these recordings on medium spiny neurons from the striatum, granule cells from the HpDG, and thalamic neurons. The holding potential was set at -70 mV, and pipette resistance typically ranged from 5~8 MΩ. The pipettes were filled with an internal solution composed of (in mM) 135 CsCl, 4 NaCl, 0.5 $CaCl_2$, 10 HEPES, 5 EGTA, 30 QX-314; the pH was adjusted to 7.2 with CsOH (278~285 mOsmol/kg). This solution measured inhibitory postsynaptic currents (IPSCs) and tonic currents. IPSCs and tonic currents were measured in the presence of ionotropic glutamate receptor antagonists: 50 μM D-2-amino-5-phosphonovalerate (APV, Tocris) and 20 μM cyanquixaline (CNQX, Tocris). The amplitude of $GABA_A$ receptor ($GABA_AR$)-mediated current was measured by observing baseline shifts following the bath application of 50 μM (-)-bicuculline methobromide (BIC, Tocris) in the striatum, HpDG; 50 μM gabazine (GBZ, Tocris) in the Pf. The amplitude of activated extrasynaptic $GABA_AR$ currents was assessed by comparing baseline shifts before and after the application of 5 μM GABA or 2 μM 4,5,6,7-Tetrahydroisoxazolo[5,4-*c*] pyridin-3-ol hydrochloride (THIP, Tocris), and 50 μM BIC or 50 μM GBZ. The current shifts were measured using 5 μM GABA and 50 μM BIC in the striatum, 2 μM THIP and 50 μM BIC in the HpDG, and 5 μM GABA with 50 μM GBZ in the Pf. Data were filtered at 2 kHz and analyzed for amplitude and frequency of spontaneous IPSC (sIPSC) using Minianalysis software (Bluecell).

Statistical analysis

The Shapiro-Wilcoxon normality test was used for data normality in all experiments. If data follows a normal distribution, an unpaired two-tailed t-test was used to determine the differences between the groups. Otherwise, a Mann-Whitney test (two-tailed) was used. The significance level is represented as asterisks (*$p<0.05$, **$p<0.01$, ***$p<0.001$, ****$p<0.0001$: non-significancy shown as p-value). GraphPad Prism 10.2.3 for Windows (GraphPad Software, USA) was used for data analysis and plotting. The median value was mentioned in the Mann-Whitney test, and the mean value was mentioned in the unpaired t-test.

RESULTS

Generation of Best1 floxed mouse line and BEST1 aKO mouse line

The *Best1* gene is located on the positive strand of chromosome 19 (19q) of *Mus musculus* (NC_000085.7), spanning 9,962,538 to 9,978,997, and comprises 12 exons. During the generation of the *Best1* floxed mouse, the *Best1* floxed allele was produced using the traditional ES cell targeting method commonly employed in mouse model gene engineering. Mouse genomic fragments, including homology arms, loxP sequences, and target exons, were amplified and recombined using a BAC clone. The recombined target vector was introduced into ES cells via electroporation and resulted in the generation of the *Best1* floxed allele through homology-directed recombination. ES cells containing the selected *Best1* floxed allele were injected into blastocysts via microinjection. After screening with a selective marker, these selected ES cells were transferred to pseudopregnant females. The delivered chimeric mice were bred with wild-type (WT) mice, obtaining mice heterozygous for the *Best1* floxed allele (Fig. 1A, B). Subsequently, the obtained *Best1* floxed mice (C57BL/6JCya-*Best1*^{em1flox}/Cya) were genotyped using two primer pairs to confirm the presence of loxP sequences upstream of exon 3 and downstream of exon 6. Pair 1, using Forward #1 (F1) and Reverse #1 (R1) primers for the loxP sequence downstream of exon 6, identified three genotypes: a single 283 bp band for homozygous (fl/fl), two bands at 283 and 187 bp for heterozygous (fl/+), and a single 187 bp band for wildtype (+/+). Pair 2, using Forward #2 (F2) and Reverse #2 (R2) primers for the loxP sequence upstream of exon 3, similarly identified three genotypes: a single 259 bp band for homozygous (fl/fl), two bands at 259 and 226 bp for heterozygous (fl/+), and a single 226 bp band for wildtype (+/+). The genotyping protocol was adapted and modified to distinguish between three genotypes: two bands at 439 and 179 bp for homozygous (Cre/Cre), three bands at 439, 256, and 179 bp for heterozygous (Cre/+), and a single 256

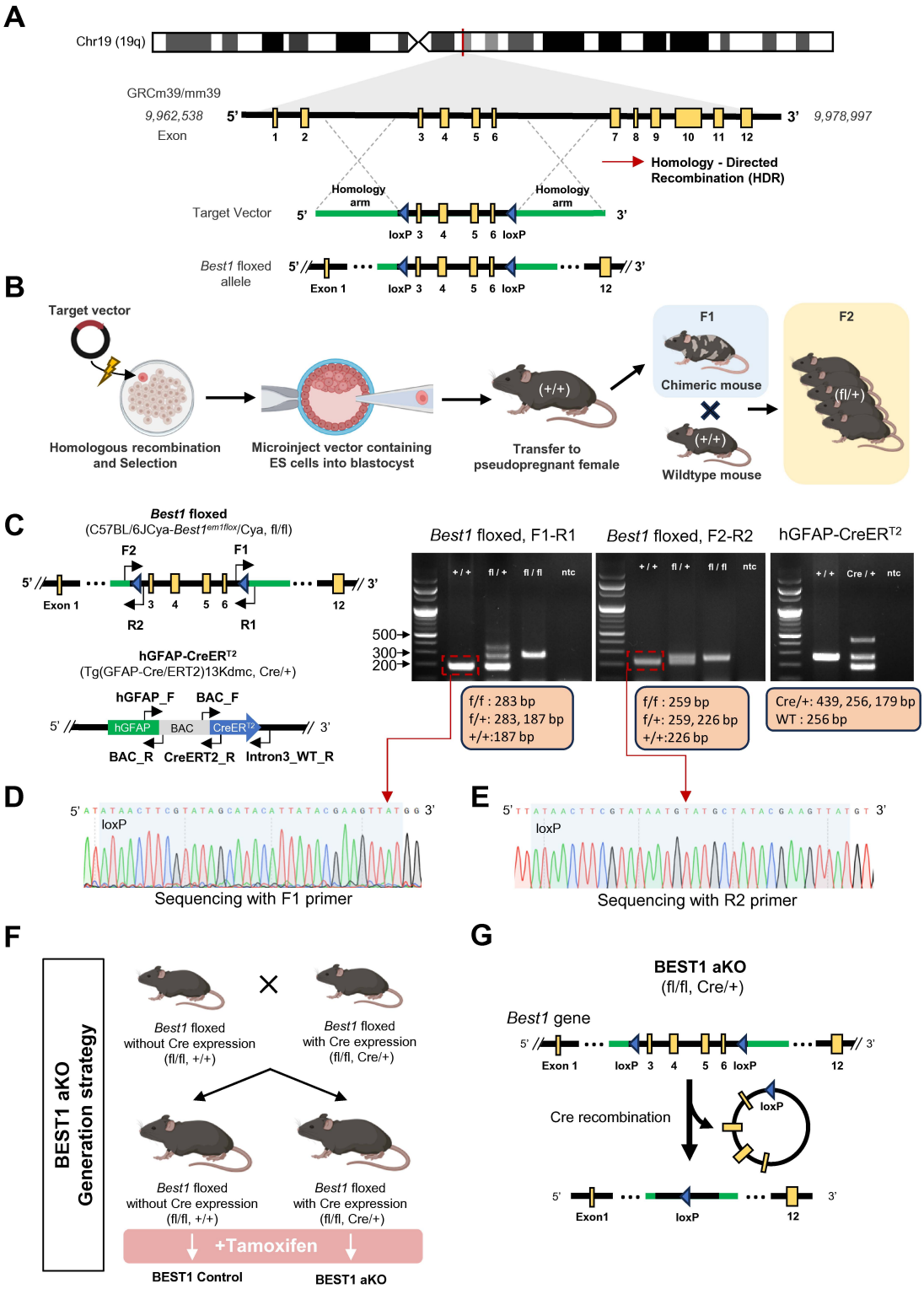

Fig. 1. Generation of *Best1* floxed mouse line and BEST1 aKO mouse line. (A) Schematic illustration of generating heterozygous *Best1* floxed mouse using ES cell targeting method. (B) Schematic diagram of *Best1* gene location in chromosome 19 (top) and generation of *Best1* floxed allele using homology-directed recombination. (C) (left) Construct of *Best1* floxed allele in *Best1* floxed mouse (C57BL/6JCya-*Best1*^{em1flox}/Cya, fl/fl) with two sets of primer for genotyping (F1-R1, F2-R2). (right) Genotyping result using F1-R1, F2-R2, and primers for hGFAP-CreER^{T2} mouse. (bottom) Band size information for determining genotypes. (D) Sequencing results of loxP sites (blue highlighted) upstream of exon 3 using F1 primer. (E) Sequencing results of loxP site (blue highlighted) downstream of exon 6 using R2 primer. (F) Schematic diagram of BEST1 aKO generation strategy specific to mating. (G) Schematic diagram of knocking out *Best1* gene by Cre recombination.

https://doi.org/10.5607/en24019

bp band for wildtype (+/+) [28]. In this study, however, we applied this method but focused exclusively on using heterozygous and wildtype mice (Fig. 1C). Sanger sequencing using F1 and R2 primers confirmed that the loxP sequences downstream and upstream of the *Best1* floxed allele were fully intact, spanning the original 34 bp (Fig.1D, E). Subsequently, to generate BEST1 aKO mice, *Best1* floxed mice were bred with hGFAP-CreER^{T2} mice to produce *Best1* floxed/ hGFAP-CreER^{T2} mice. To maintain homozygosity in the *Best1* floxed alleles and generate experimental groups based on Cre expression, homozygous *Best1* floxed mice without Cre expression (fl/fl, +/+) were bred with homozygous *Best1* floxed mice with Cre expression (fl/fl, Cre/+) (Fig. 1F). Both mouse genotype group (fl/fl, +/+; fl/fl, Cre/+) were injected with tamoxifen (100 mg/kg) once daily for five days by intraperitoneal route. CreER^{T2} translocation to the nucleus causes recombination of loxP-flanked exons 3 and 6 under the control of human GFAP promoter, generating BEST1 aKO mice (Fig. 1G).

BEST1 aKO mice show a significant reduction in GABA content, BEST1 expression in astrocytes, and tonic GABA current in the striatum

Previously, we have reported that BEST1 mediates the tonic release of GABA, which is synthesized mainly by MAOB in the striatum astrocytes [5]. In this study, we investigate the levels of BEST1 and GABA in astrocytes within the striatum of BEST1 control (fl/fl, +/+) and BEST1 aKO (fl/fl, Cre/+) mice. To measure the difference between the two groups, both *Best1* floxed/hGFAP-CreER^{T2} mice genotype group were injected with 100 mg /kg /day tamoxifen five days a row to induce astrocytic ablation of BEST1, as previously validated [28]. After 2~3 weeks later, IHC and electrophysiology experiment were conducted (Fig. 2A, B). In IHC, we performed immunostaining against S100β, GABA, and BEST1. Immunostaining small molecules like GABA has been confirmed by directly correlating the amount of GABA and the degree of tonic inhibition [29] and a positive correlation between GABA content and immunostaining intensity [30].

We observed colocalization of GABA and BEST1 within S100β-positive cell area, highlighted with a white arrow (Fig. 2C). There is significant GABA and BEST1 reduction in the S100β-positive cell area of BEST1 aKO mouse compared to BEST1 control (Fig. 2D). To check the contribution of astrocytic BEST1 channel to the tonic GABA level of the striatum, we measure tonic GABA current in the medial spiny neurons (MSNs) (Fig. 2B). Under treatment of AMPA receptor (AMPAR) and NMDA receptor (NMDAR) blockers, CNQX, and APV, $GABA_A$R-mediated tonic GABA current (I_{Tonic}) was measured as a shift of current between baseline and application of $GABA_A$R antagonist, BIC (50 μM). The GABA-induced current (I_{GABA}) was calculated as the current difference between the peak following GABA (5 μM) application and the observed after treatment with BIC (Fig. 2E). Tonic GABA current was significantly decreased by 66.7% in BEST1 aKO compared to BEST1 control. At the same time, there is no significant change in GABA-induced current, membrane capacitance (Cm), sIPSC amplitude, and frequency (Fig. 2F~H). This result suggests that astrocyte-specific BEST1 majorly contributes to tonic GABA release in the striatum.

BEST1 aKO mice show a significant reduction in BEST1 expression and tonic GABA current, along with increased GABA content in astrocytes in the HpDG

Tonic GABA-mediated inhibition has also been reported in the HpDG [21], as seen in the striatum [21]. To assess the differences in BEST1 and GABA levels between the two groups, the expression of BEST1 and GABA was compared in HpDG of BEST1 control and BEST1 aKO mice through IHC. The experiment timeline in HpDG was the same as in the striatum (Fig. 3A). In IHC data, colocalization of GABA and BEST1 with S100β-positive cell area, highlighted with a white arrow, was observed (Fig. 3C). In the S100β-positive cell areas of BEST1 aKO mice compared to BEST1 control mice, there was a significant reduction in BEST1 expression; however, BEST1 aKO showed significantly increased GABA content in astrocytes (Fig. 3D). To check the contribution of astrocytic BEST1 channel for tonic inhibition in HpDG, we measure the tonic GABA current of the granule cell (Fig. 3B). In the presence of CNQX and APV, $GABA_A$R-mediated tonic GABA current was measured by application of BIC (50 μM). It has been reported that the HpDG exhibits a dense expression of the $GABA_A$R δ-subunit [30], which is known to localize at extrasynaptic and perisynaptic sites [31], showing high sensitivity to THIP [30, 32]. We observed that several papers have treated THIP or GABA in a dose-dependent manner to compare extrasynaptic $GABA_A$R activation, focusing primarily on changes in δ-subunit activation due to different pharmacological treatments [33-35]. However, due to the scarcity of studies that focus exclusively on the activation of extrasynaptic $GABA_A$R by THIP in the HpDG of genetically engineered mouse lines, there is a need to investigate these currents, specifically in the *Best1* aKO mouse. Therefore, the $GABA_A$R δ-subunit agonist, THIP (2 μM), was used to selectively activate extrasynaptic $GABA_A$R in the HpDG of BEST1 aKO mouse (Fig. 3E). Tonic GABA current was significantly decreased by 46.4% in BEST1 aKO compared to BEST1 control. At the same time, there is no significant change in THIP-induced current, Cm, sIPSC amplitude, and frequency (Fig. 3F~H). This result implicates that astrocyte-specific BEST1 is majorly contributing to tonic GABA

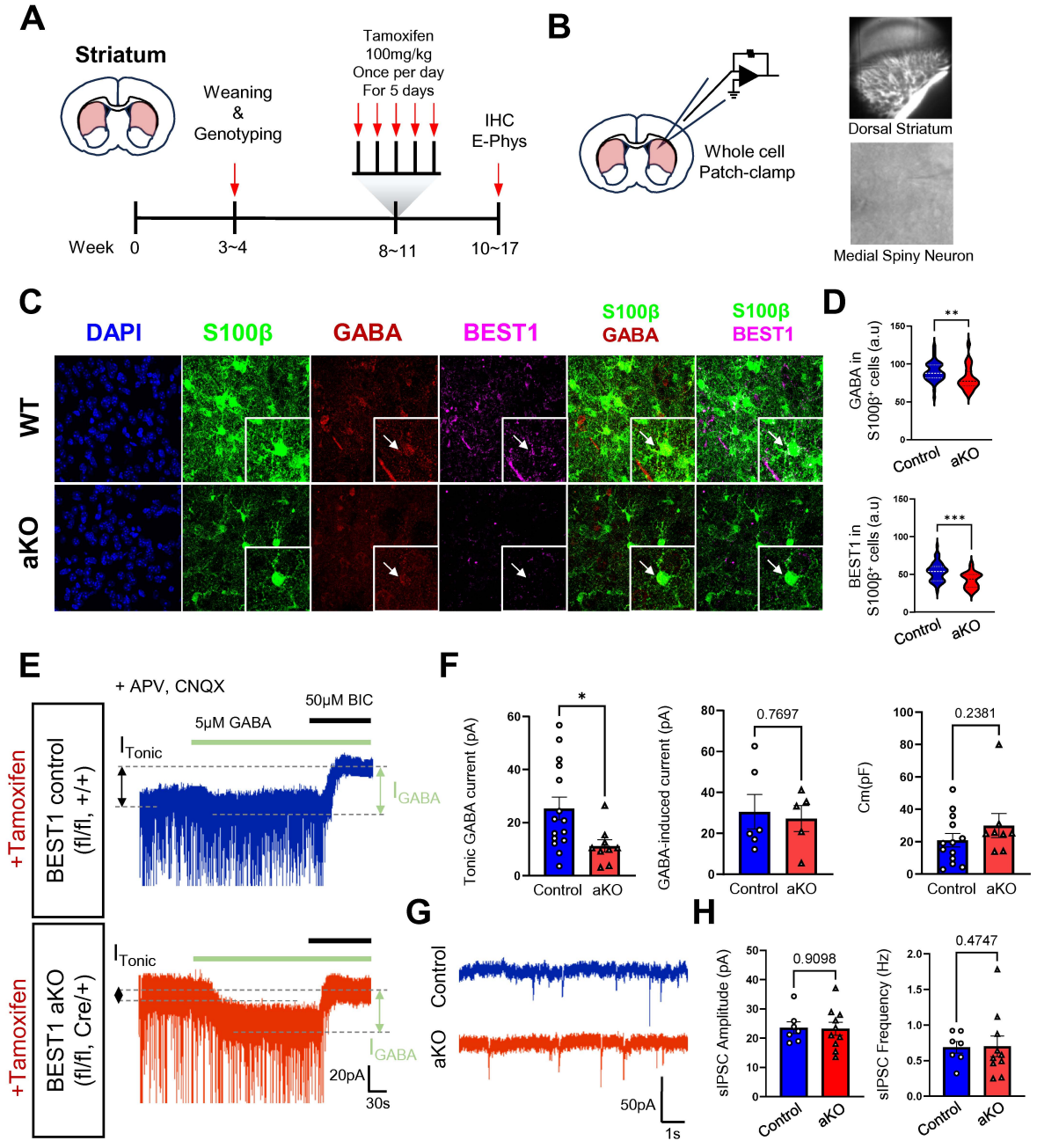

Fig. 2. BEST1 aKO mice show a significant reduction in GABA content, BEST1 expression in astrocytes, and tonic GABA current in the striatum. (A) Experimental scheme and timeline of generating and using BEST1 aKO mouse. (B) Schematic diagram of the striatum in the coronal plane of *Best1* floxed/hGFAP-CreER^{T2} mouse (left) and DIC image of a whole cell-patch clamped region in the dorsal striatum and medial spiny neuron (right). (C) Representative confocal images of DAPI (blue), S100β (green), GABA (red), and BEST1 (Magenta) in the coronal plane of dorsal striatum from BEST1 control and BEST1 aKO mouse. The white box is a magnified image. (D) (top) Violin plot showing GABA intensity in S100β-positive cells in the striatum (control: 87.99; aKO: 77.48; Mann-Whitney test, p=0.0021). (bottom) Violin plot for BEST1 intensity in S100β-positive cells (control: 53.64; aKO: 42.43; unpaired t-test, p=0.0002). (E) Representative traces from tamoxifen-injected BEST1 control (without Cre expression) and BEST1 aKO (with Cre expression). Measured currents include GABA-induced current (I_{GABA}, green arrow) and ambient tonic GABA current (I_{Tonic}, black arrow) after serial bath application of 5 μM GABA (green line) and 50 μM BIC (black line). (F) Summarized scatter bar graphs of ambient tonic GABA current, GABA-induced current, and Cm (left, control, 25.36, aKO, 11.21, unpaired t-test, p=0.0232) (middle, control, 30.56, aKO, 27.26, unpaired t-test, p= 0.7697) (right, control, 19.03, aKO, 25.08, Mann-Whitney test, p=0.2381). (G) Representative trace of sIPSC from BEST1 control and BEST1 aKO mouse. (H) Summarized scatter bar graphs of sIPSC amplitude and sIPSC frequency. (left, control, 23.56, aKO, 23.20, unpaired t-test, p=0.9098) (right, control, 0.7420, aKO, 0.5580, Mann-Whitney test, p=0.4747).

https://doi.org/10.5607/en24019

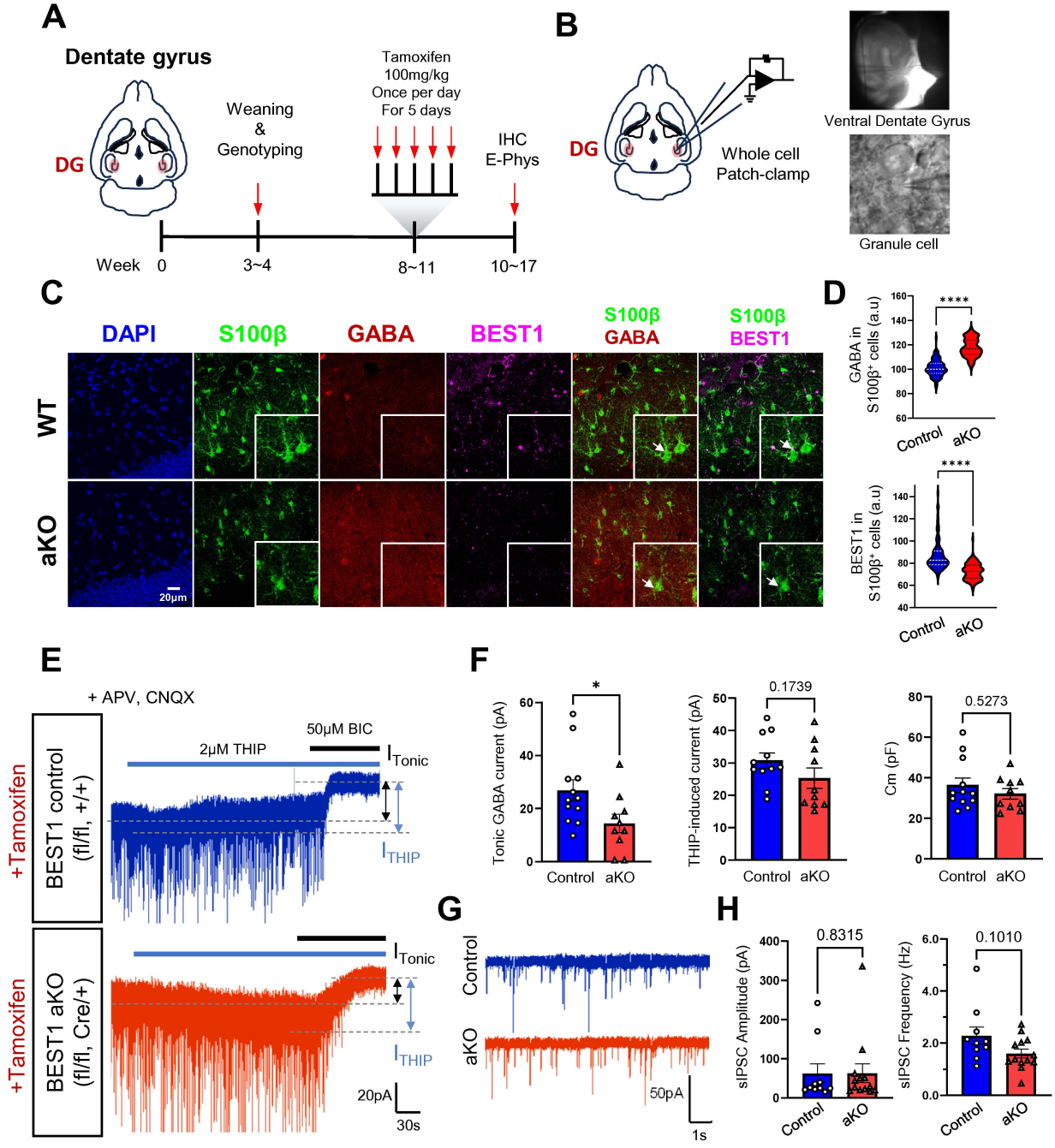

Fig. 3. BEST1 aKO mice show a significant reduction in BEST1 expression and tonic GABA current, along with increased GABA content in astrocytes in the HpDG. (A) Experimental scheme and timeline of generating and using BEST1 aKO mouse. (B) Schematic diagram of HpDG in the horizontal plane of *Best1* floxed/hGFAP-CreER^{T2} mouse (left) and DIC image of a whole cell-patch clamped region in the ventral dentate gyrus and granule cells (right). (C) Representative confocal images of DAPI (blue), S100β (green), GABA (red), and BEST1 (Magenta) in the coronal plane of HpDG from BEST1 control and BEST1 aKO mouse. The white box is a magnified image. (D) (left) Violin plot showing GABA intensity in S100β-positive cells in the HpDG (control, 100.2, aKO, 116.9, Mann-Whitney test, p<0.0001). (middle) Violin plot for BEST1 intensity in S100β-positive cells (control, 82.77, aKO, 72.78, Mann-Whitney test, p<0.0001). (E) Representative traces from tamoxifen-injected BEST1 control (without Cre expression) and BEST1 aKO (with Cre expression). Measured currents include THIP-induced current (I_{THIP}, blue arrow) and ambient tonic GABA current (I_{Tonic}, black arrow) after serial bath application of 2 μM THIP (blue line) and 50 μM BIC (black line). (F) Summarized scatter bar graphs of ambient tonic GABA current, THIP-induced current, and Cm value (left, control, 26.88, aKO, 14.42, unpaired t-test, p=0.0313) (middle, control, 30.77, aKO, 25.28, unpaired t-test, p=0.1739) (right, control, 32.44, aKO, 30.59, Mann-Whitney test, p=0.5273). (G) Representative trace of sIPSC from BEST1 control and BEST1 aKO mouse. (H) Summarized scatter bar graphs of sIPSC amplitude and sIPSC frequency (left, control, 26.14, aKO, 28.88, Mann-Whitney test, p=0.8315) (right, control, 2.041, aKO, 1.374, Mann-Whitney test, p=0.1010).

release in HpDG.

BEST1 aKO mice show a significant reduction in BEST1 expression, tonic GABA current, and increased GABA content in astrocytes in the Pf

We have presented that tonic release of astrocytic GABA via the BEST1 channel controls sensory acuity in thalamic ventrobasal region (VB) [8]. To assess the differences in BEST1 and GABA levels between BEST1 control and BEST1 aKO mice, we compared the expression of BEST1 and GABA in the Pf of the two groups using IHC. The experimental timeline in the Pf was the same as in the striatum, and HpDG (Fig. 4A). Brain slices were immunostained for S100β, GABA, and BEST1. Under confocal microscopy, colocalization of GABA and BEST1 within the S100β-positive cell area was observed, highlighted with a white arrow (Fig. 4C). In the S100β-positive cell areas of BEST1 aKO mice compared to BEST1 control mice, there was a significant reduction in BEST1 expression; however, significantly increased GABA content in astrocytes was identified, similar with HpDG (Fig. 4D). In addition, as we have reported neuronal BEST1 expression in thalamic reticular neurons [36], we have also examined neuronal BEST1 and found that there was no significant change in BEST1 level in BEST1-positive thalamocortical neurons (highlighted with yellow arrow) between BEST1 control and BEST1 aKO (Fig. 4C). This result indicates astrocyte-specific removal of BEST1 in BEST1 aKO mice. To determine if astrocytic BEST1 is required for tonic inhibition in the Pf, we measured the tonic GABA current in thalamocortical neurons (Fig. 4B). In the presence of CNQX and APV, $GABA_A$R-mediated tonic GABA current was assessed using another allosteric $GABA_A$R antagonist, GBZ (50 μM) [37]. The tonic GABA current was significantly decreased by 49.6% in BEST1 aKO mice compared to BEST1 control mice. At the same time, there was no significant change in GABA-induced current, Cm, or sIPSC amplitude and frequency (Fig. 4F~H). These results suggest that astrocyte-specific BEST1 significantly contributes to Pf's tonic GABA release.

DISCUSSION

To date, the reported BEST1 null KO mouse line has been on a Balb/c background [38], and this mouse line has not been sufficient for studying astrocytic BEST1. Recognizing the importance of astrocytic BEST1 in various gliotransmission research through previous reports[4, 15, 16], we successfully generated *Best1* floxed (C57BL/6JCya-*Best1*^{em1flox}/Cya) using the ES cell targeting method. We crossed these with hGFAP-CreER^{T2} mice to generate BEST1 aKO mice. Using the CreER^{T2} system allows us to control the time window of Cre recombinase activation by injecting tamoxifen. This system enables us to ablate a developmentally important gene without fatal underdevelopment. Consistent with previous studies [5, 8, 21], ablation of astrocytic BEST1 showed a critical reduction in tonic inhibition by 66.7% in the striatum, 46.4% in the HpDG, and 49.6% in the Pf, compared to Cre-negative controls, without affecting phasic inhibition (Fig. 5).

Due to its low expression level of GFAP (https://www.proteinatlas.org/ENSG00000131095-GFAP/brain), It is well established that GFAP promoter does not work well in the striatum and thalamus. To overcome the limitation due to the low expression level of GFAP, GLAST-CreER^{T2} [39] and ALDH1L1-CreER^{T2} [40] mouse lines have been developed. However, the Glast-CreER^{T2} mouse line exhibits significant neuronal expression, and the Aldh1l1-CreER^{T2} line is not ideal for brain-specific targeting due to its expression in other body parts [27]. In a previous study validating the hGFAP-CreER^{T2} mouse [28], we assessed astrocyte specificity (tdTomato+ & S100β+/tdTomato+) and coverage (tdTomato+ & S100β+/S100β+) in brain sections from the hGFAP-CreER^{T2}×Ai14 double transgenic mouse line using S100β immunostaining. The striatum showed high astrocyte specificity (89%) but moderate coverage (50%), whereas the thalamic VB area demonstrated moderate astrocyte specificity (64%) and high coverage (89%). Our measurements indicated reductions in tonic GABA current of 66.7% in the striatum and 49.6% in the thalamus. The decrease in tonic GABA current appears to be correlated with astrocyte specificity. These results confirm that the GFAP promoter functions effectively in both the striatal and thalamic regions. Our measurements demonstrated a reduction in tonic GABA currents of 66.7% in the striatum and 49.6% in the Pf. This decrease in tonic GABA current is seemingly correlated with astrocytic specificity. Consequently, aligning our tonic GABA current reduction data with the previously reported high astrocytic specificity in the hGFAP-CreER^{T2}×Ai14 double transgenic mouse line substantiates the reliability of the Cre-expression system of hGFAP-CreER^{T2} in the striatum and thalamus.

In the Best1 aKO mouse immunostaining data, we observed that the BEST1 level significantly decreased. We expected unreleased GABA can be accumulated in the astrocyte since GABA can be released through the BEST1 channel. GABA level was significantly increased in the HpDG and Pf. However, GABA expression was paradoxically decreased in the striatum. The high level of GABA degradation enzyme, ABAT, expression in the striatum can explain this paradoxical decrease of GABA. However, there is a lack of evidence on whether striatal astrocytes express high levels of ABAT. Therefore, future investigation is needed to determine the astrocytic ABAT level in the striatum.

https://doi.org/10.5607/en24019

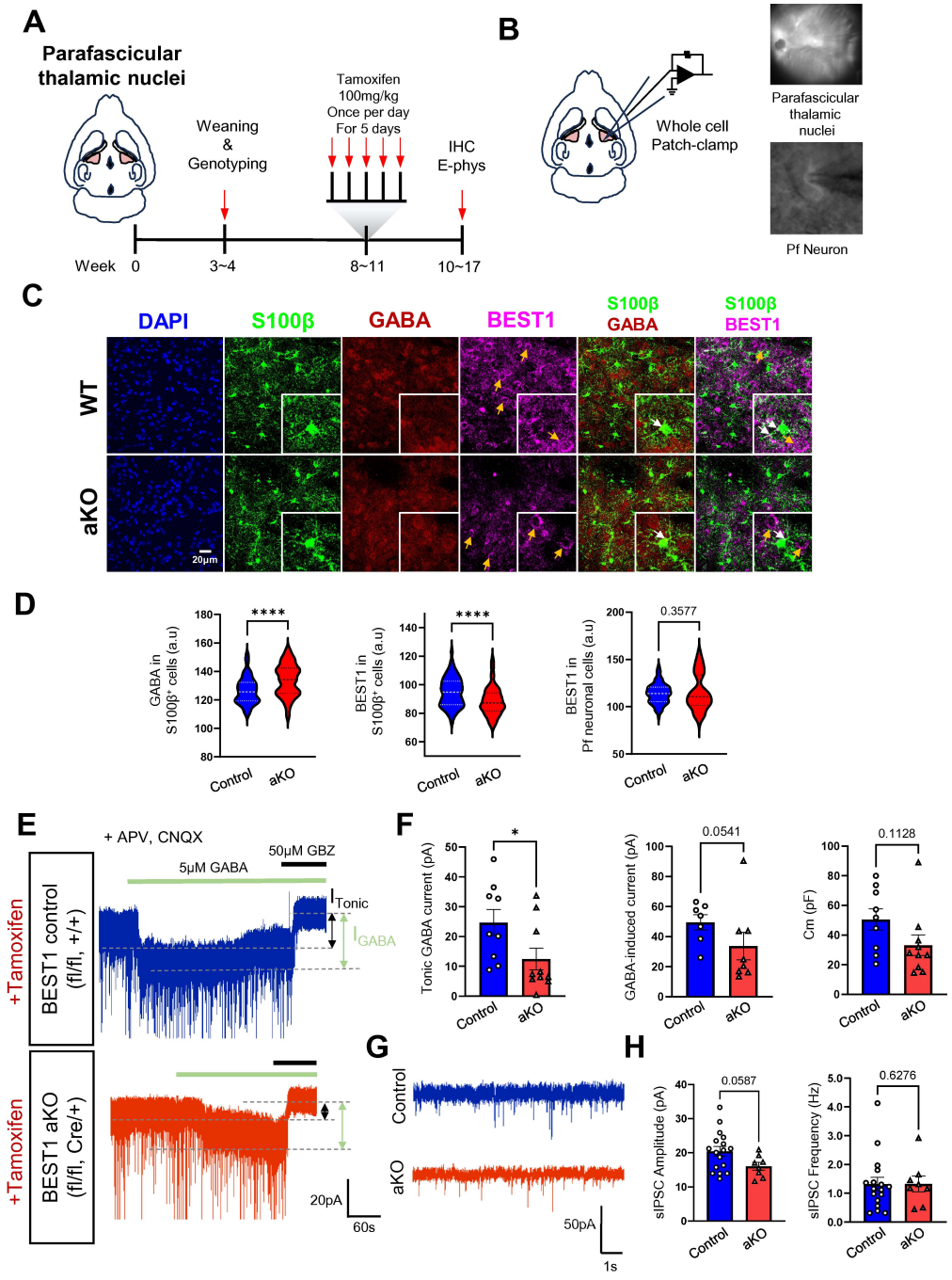

Fig. 4. BEST1 aKO mice show a significant reduction in BEST1 expression, tonic GABA current, and increased GABA content in astrocytes in the Pf. (A) Experimental scheme and timeline of generating and using BEST1 aKO mouse. (B) Schematic diagram of the Pf in the horizontal plane of *Best1* floxed/hGFAP-CreER^{T2} mouse (left) and DIC image of a whole cell-patch clamped region in the Pf and Pf neuron (right). (C) Representative confocal images of DAPI (Blue), S100β (Green), GABA (Red), and BEST1 (Magenta) in the coronal plane of the Pf from BEST1 control and BEST1 aKO mouse. The white box is a magnified image. (D) (left) Violin plot showing GABA intensity in S100β-positive cells in the Pf (control, 125.8, aKO, 134.3, Mann-Whitney test, p<0.0001). (middle) Violin plot for BEST1 intensity in S100β-positive cells (control, 95.00, aKO, 87.30, Mann-Whitney test, p<0.0001). (right) Violin plot for BEST1 intensity in Pf neuronal cells (control, 114.1, aKO, 110.8, Mann-Whitney test, p=0.3577). (E) Representative traces from tamoxifen-injected BEST1 control (without Cre expression) and *Best1* aKO (with Cre expression). Measured currents include GABA-induced current (I_{GABA}, green arrow) and ambient tonic GABA current (I_{Tonic}, black arrow) after serial bath application of 5 μM GABA (green line) and 50 μM GBZ (black line). (F) Summarized scatter bar graphs of ambient tonic GABA current, GABA-induced current, and Cm (left, control, 20.81, aKO, 6.912, Mann-Whitney test, p=0.0220) (middle, control, 53.92, aKO, 22.73, Mann-Whitney test, p=0.0541) (right, control, 51.88, aKO, 27.21, Mann-Whitney test, p=0.1128). (G) Representative trace of sIPSC from BEST1 control and BEST1 aKO mouse. (H) Summarized scatter bar graphs of sIPSC amplitude and sIPSC frequency (left, control, 20.43, aKO, 16.05, unpaired t-test, p=0.0587) (right, control, 1.159, aKO, 1.242, Mann-Whitney test, p=0.6276).

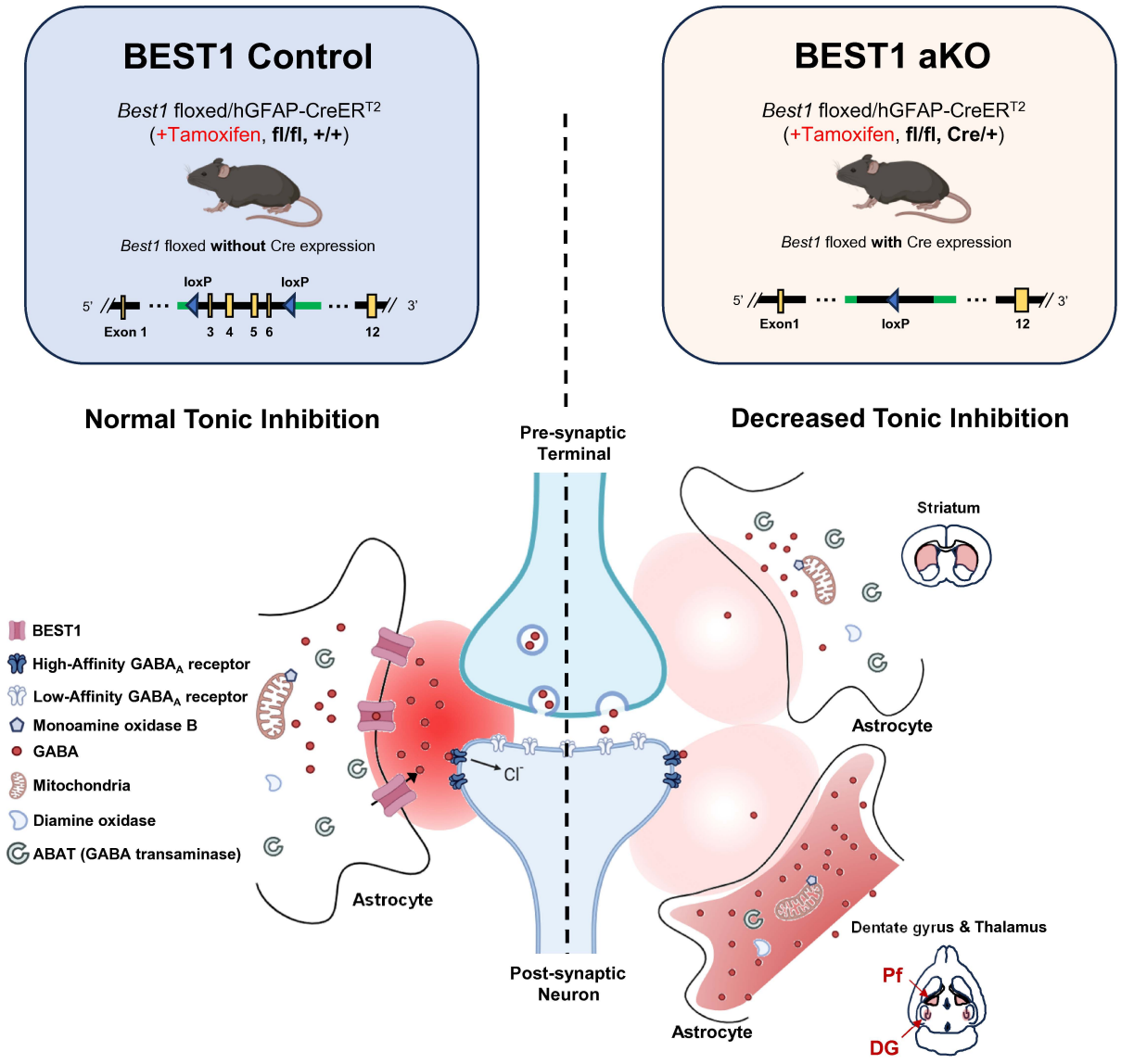

Fig. 5. Schematic illustration of generation (top) and characterization (bottom) of astrocyte-specific Best conditional KO (BEST1 aKO) mice. BEST1 aKO mice show reduced tonic GABA inhibition with reduced levels of BEST1 expression in astrocytes, compared to Cre-negative control.

Additionally, the BEST1 channel mediates slow glutamate release in astrocytes upon GPCR activation [13] and, along with the co-release of D-serine [16], contributes to tonic NMDAR currents in the hippocampus [16, 41]. The BEST1 aKO mouse will help study both glutamate release and the contribution of BEST1 to the tonic NMDAR current in the brain. This mouse line will be valuable for future studies on GABA and other gliotransmitters, such as glutamate and D-serine, mediated by astrocytic BEST1.

ACKNOWLEDGEMENTS

The Institute for Basic Science Center for Cognition and Sociality (IBS-R001-D2-2024-a00) supported this research for C.J.L.

REFERENCES

1. Marmorstein AD, Marmorstein LY, Rayborn M, Wang X, Hollyfield JG, Petrukhin K (2000) Bestrophin, the product of the Best vitelliform macular dystrophy gene (VMD2), localizes to the basolateral plasma membrane of the retinal pigment epithelium. Proc Natl Acad Sci U S A 97:12758-12763.
2. Johnson AA, Guziewicz KE, Lee CJ, Kalathur RC, Pulido JS, Marmorstein LY, Marmorstein AD (2017) Bestrophin 1 and retinal disease. Prog Retin Eye Res 58:45-69.

3. Oh SJ, Lee CJ (2017) Distribution and function of the bestrophin-1 (Best1) channel in the brain. Exp Neurobiol 26:113-121.
4. Lee S, Yoon BE, Berglund K, Oh SJ, Park H, Shin HS, Augustine GJ, Lee CJ (2010) Channel-mediated tonic GABA release from glia. Science 330:790-796.
5. Yoon BE, Woo J, Chun YE, Chun H, Jo S, Bae JY, An H, Min JO, Oh SJ, Han KS, Kim HY, Kim T, Kim YS, Bae YC, Lee CJ (2014) Glial GABA, synthesized by monoamine oxidase B, mediates tonic inhibition. J Physiol 592:4951-4968.
6. Park H, Han KS, Oh SJ, Jo S, Woo J, Yoon BE, Lee CJ (2013) High glutamate permeability and distal localization of Best1 channel in CA1 hippocampal astrocyte. Mol Brain 6:54.
7. Oh SJ, Han KS, Park H, Woo DH, Kim HY, Traynelis SF, Lee CJ (2012) Protease activated receptor 1-induced glutamate release in cultured astrocytes is mediated by bestrophin-1 channel but not by vesicular exocytosis. Mol Brain 5:38.
8. Kwak H, Koh W, Kim S, Song K, Shin JI, Lee JM, Lee EH, Bae JY, Ha GE, Oh JE, Park YM, Kim S, Feng J, Lee SE, Choi JW, Kim KH, Kim YS, Woo J, Lee D, Son T, Kwon SW, Park KD, Yoon BE, Lee J, Li Y, Lee H, Bae YC, Lee CJ, Cheong E (2020) Astrocytes control sensory acuity via tonic inhibition in the thalamus. Neuron 108:691-706.e10.
9. Al-Jumaily M, Kozlenkov A, Mechaly I, Fichard A, Matha V, Scamps F, Valmier J, Carroll P (2007) Expression of three distinct families of calcium-activated chloride channel genes in the mouse dorsal root ganglion. Neurosci Bull 23:293-299.
10. André S, Boukhaddaoui H, Campo B, Al-Jumaily M, Mayeux V, Greuet D, Valmier J, Scamps F (2003) Axotomy-induced expression of calcium-activated chloride current in subpopulations of mouse dorsal root ganglion neurons. J Neurophysiol 90:3764-3773.
11. Pineda-Farias JB, Barragán-Iglesias P, Loeza-Alcocer E, Torres-López JE, Rocha-González HI, Pérez-Severiano F, Delgado-Lezama R, Granados-Soto V (2015) Role of anoctamin-1 and bestrophin-1 in spinal nerve ligation-induced neuropathic pain in rats. Mol Pain 11:41.
12. Woo J, Jang MW, Lee J, Koh W, Mikoshiba K, Lee CJ (2020) The molecular mechanism of synaptic activity-induced astrocytic volume transient. J Physiol 598:4555-4572.
13. Woo DH, Han KS, Shim JW, Yoon BE, Kim E, Bae JY, Oh SJ, Hwang EM, Marmorstein AD, Bae YC, Park JY, Lee CJ (2012) TREK-1 and Best1 channels mediate fast and slow glutamate release in astrocytes upon GPCR activation. Cell 151:25-40.
14. Lee JM, Gadhe CG, Kang H, Pae AN, Lee CJ (2022) Glutamate permeability of chicken Best1. Exp Neurobiol 31:277-288.
15. Han KS, Woo J, Park H, Yoon BJ, Choi S, Lee CJ (2013) Channel-mediated astrocytic glutamate release via bestrophin-1 targets synaptic NMDARs. Mol Brain 6:4.
16. Koh W, Park M, Chun YE, Lee J, Shim HS, Park MG, Kim S, Sa M, Joo J, Kang H, Oh SJ, Woo J, Chun H, Lee SE, Hong J, Feng J, Li Y, Ryu H, Cho J, Lee CJ (2022) Astrocytes render memory flexible by releasing D-serine and regulating NMDA receptor tone in the hippocampus. Biol Psychiatry 91:740-752.
17. Koh W, Kwak H, Cheong E, Lee CJ (2023) GABA tone regulation and its cognitive functions in the brain. Nat Rev Neurosci 24:523-539.
18. Woo J, Min JO, Kang DS, Kim YS, Jung GH, Park HJ, Kim S, An H, Kwon J, Kim J, Shim I, Kim HG, Lee CJ, Yoon BE (2018) Control of motor coordination by astrocytic tonic GABA release through modulation of excitation/inhibition balance in cerebellum. Proc Natl Acad Sci U S A 115:5004-5009.
19. Chun H, Im H, Kang YJ, Kim Y, Shin JH, Won W, Lim J, Ju Y, Park YM, Kim S, Lee SE, Lee J, Woo J, Hwang Y, Cho H, Jo S, Park JH, Kim D, Kim DY, Seo JS, Gwag BJ, Kim YS, Park KD, Kaang BK, Cho H, Ryu H, Lee CJ (2020) Severe reactive astrocytes precipitate pathological hallmarks of Alzheimer's disease via H_2O_2- production. Nat Neurosci 23:1555-1566.
20. Heo JY, Nam MH, Yoon HH, Kim J, Hwang YJ, Won W, Woo DH, Lee JA, Park HJ, Jo S, Lee MJ, Kim S, Shim JE, Jang DP, Kim KI, Huh SH, Jeong JY, Kowall NW, Lee J, Im H, Park JH, Jang BK, Park KD, Lee HJ, Shin H, Cho IJ, Hwang EM, Kim Y, Kim HY, Oh SJ, Lee SE, Paek SH, Yoon JH, Jin BK, Kweon GR, Shim I, Hwang O, Ryu H, Jeon SR, Lee CJ (2020) Aberrant tonic inhibition of dopaminergic neuronal activity causes motor symptoms in animal models of Parkinson's disease. Curr Biol 30:276-291.e9.
21. Jo S, Yarishkin O, Hwang YJ, Chun YE, Park M, Woo DH, Bae JY, Kim T, Lee J, Chun H, Park HJ, Lee DY, Hong J, Kim HY, Oh SJ, Park SJ, Lee H, Yoon BE, Kim Y, Jeong Y, Shim I, Bae YC, Cho J, Kowall NW, Ryu H, Hwang E, Kim D, Lee CJ (2014) GABA from reactive astrocytes impairs memory in mouse models of Alzheimer's disease. Nat Med 20:886-896.
22. Park H, Oh SJ, Han KS, Woo DH, Park H, Mannaioni G, Traynelis SF, Lee CJ (2009) Bestrophin-1 encodes for the Ca2+-activated anion channel in hippocampal astrocytes. J Neurosci 29:13063-13073.
23. Capecchi MR (2001) Generating mice with targeted mutations. Nat Med 7:1086-1090.
24. Yang L, Li H, Han Y, Song Y, Wei M, Fang M, Sun Y (2023) CRISPR/Cas9 gene editing system can alter gene expression and induce DNA damage accumulation. Genes (Basel) 14:806.

25. Pattanayak V, Ramirez CL, Joung JK, Liu DR (2011) Revealing off-target cleavage specificities of zinc-finger nucleases by in vitro selection. Nat Methods 8:765-770.
26. Mussolino C, Morbitzer R, Lütge F, Dannemann N, Lahaye T, Cathomen T (2011) A novel TALE nuclease scaffold enables high genome editing activity in combination with low toxicity. Nucleic Acids Res 39:9283-9293.
27. Petryszak R, Keays M, Tang YA, Fonseca NA, Barrera E, Burdett T, Füllgrabe A, Fuentes AM, Jupp S, Koskinen S, Mannion O, Huerta L, Megy K, Snow C, Williams E, Barzine M, Hastings E, Weisser H, Wright J, Jaiswal P, Huber W, Choudhary J, Parkinson HE, Brazma A (2016) Expression Atlas update--an integrated database of gene and protein expression in humans, animals and plants. Nucleic Acids Res 44:D746-D752.
28. Park YM, Chun H, Shin JI, Lee CJ (2018) Astrocyte Specificity and Coverage of hGFAP-CreERT2 [Tg(GFAP-Cre/ERT2)13Kdmc] mouse line in various brain regions. Exp Neurobiol 27:508-525.
29. Lee CJ, Yoon BE (2014) Protease-activated receptor 1-induced GABA release in cultured cortical astrocytes pretreated with GABA is mediated by the bestrophin-1 channel. Anim Cells Syst (Seoul) 18:244-249.
30. Hörtnagl H, Tasan RO, Wieselthaler A, Kirchmair E, Sieghart W, Sperk G (2013) Patterns of mRNA and protein expression for 12 GABAA receptor subunits in the mouse brain. Neuroscience 236:345-372.
31. Brickley SG, Mody I (2012) Extrasynaptic GABA(A) receptors: their function in the CNS and implications for disease. Neuron 73:23-34.
32. Chandra D, Jia F, Liang J, Peng Z, Suryanarayanan A, Werner DF, Spigelman I, Houser CR, Olsen RW, Harrison NL, Homanics GE (2006) GABAA receptor α4 subunits mediate extrasynaptic inhibition in thalamus and dentate gyrus and the action of gaboxadol. Proc Natl Acad Sci U S A 103:15230-15235.
33. Trent S, Hall J, Connelly WM, Errington AC (2019) Cyfip1 haploinsufficiency does not alter $GABA_A$ receptor δ-subunit expression and tonic inhibition in dentate gyrus PV^+ interneurons and granule cells. eNeuro 6:ENEURO.0364-18.2019.
34. Carver CM, Reddy DS (2013) Neurosteroid interactions with synaptic and extrasynaptic GABA(A) receptors: regulation of subunit plasticity, phasic and tonic inhibition, and neuronal network excitability. Psychopharmacology (Berl) 230:151-188.
35. Ransom CB, Ye Z, Spain WJ, Richerson GB (2017) Modulation of tonic GABA currents by anion channel and connexin hemichannel antagonists. Neurochem Res 42:2551-2559.
36. Jung JY, Lee SE, Hwang EM, Lee CJ (2016) Neuronal expression and cell-type-specific gene-silencing of Best1 in thalamic reticular nucleus neurons using pSico-Red System. Exp Neurobiol 25:120-129.
37. Ueno S, Bracamontes J, Zorumski C, Weiss DS, Steinbach JH (1997) Bicuculline and gabazine are allosteric inhibitors of channel opening of the GABAA receptor. J Neurosci 17:625-634.
38. Marmorstein LY, Wu J, McLaughlin P, Yocom J, Karl MO, Neussert R, Wimmers S, Stanton JB, Gregg RG, Strauss O, Peachey NS, Marmorstein AD (2006) The light peak of the electroretinogram is dependent on voltage-gated calcium channels and antagonized by bestrophin (Best-1). J Gen Physiol 127:577-589.
39. Slezak M, Göritz C, Niemiec A, Frisén J, Chambon P, Metzger D, Pfrieger FW (2007) Transgenic mice for conditional gene manipulation in astroglial cells. Glia 55:1565-1576.
40. Srinivasan R, Lu TY, Chai H, Xu J, Huang BS, Golshani P, Coppola G, Khakh BS (2016) New transgenic mouse lines for selectively targeting astrocytes and studying calcium signals in astrocyte processes in situ and in vivo. Neuron 92:1181-1195.
41. Kim H, Choi S, Lee E, Koh W, Lee CJ (2024) Tonic NMDA receptor currents in the brain: regulation and cognitive functions. Biol Psychiatry 96:164-175.